Two-photon interference in optical fiber multiports

Gregor Weihs, Michael Reck, Harald Weinfurter, and Anton Zeilinger
Institut für Experimentalphysik, Universität Innsbruck, Technikerstrasse 25, A-6020 Innsbruck, Austria
(Received 14 February 1996)

We report the measurement of nonclassical photon statistics at the outputs of 2×2 and 3×3 fiber couplers resulting from quantum-mechanical second-order interference of entangled photon pairs from a parametric down-conversion source. This is a demonstration of the bunching of bosons at the outputs of fiber multiports. Single-mode fibers provide precise wavelength selection from the down-conversion source spectrum, thus yielding very long coherence times and good collection efficiency without the need of interference filters. Two-photon interference visibilities close to the theoretical maximum were achieved in the experiments. [S1050-2947(96)03307-0]

PACS number(s): 42.50.Ar, 03.65.Bz, 42.81.Qb

I. INTRODUCTION

The effect of two-photon interference on a glass plate beam splitter was demonstrated by Hong, Ou, and Mandel [1–3]. Since then some optical experiments on the foundations of quantum mechanics and quantum communications have been made with single-mode fibers [4–7]. We have measured two-photon interference at the outputs of integrated 2×2 and 3×3 fiber couplers.

Developments in fiber technology have allowed significant progress in telecommunications and made available a great number of new devices. Single-mode fiber components act on a well-defined transverse mode of the light field, thus guaranteeing high quality interference [8]. Fiber-coupled detectors give low backgrounds and good collection efficiencies. Yet some other problems, unknown to conventional optics, have to be solved. First of all it is very difficult to efficiently couple the divergent light emitted by sources with low coherence (e.g., parametric down conversion) into single-mode optical fibers. A second difficulty results from the phase instability in an optical fiber due to thermal and acoustic noise. Care must also be taken of the polarization state of light since it is changed by even slight bends in the fiber path. In the present work we show that these problems can be solved and hence optical fibers are a very good alternative to conventional ''bulk'' optics for complex interferometric setups in quantum optics.

As a source of entangled photon pairs we used the second-order nonlinear process of parametric down conversion. In a $\chi^{(2)}$-nonlinear crystal an UV photon may split spontaneously into two visible photons. Because of energy conservation their sum frequency is equal to the frequency of the pump photon. Momentum conservation in the type-I crystal leads to the emission of the down-conversion photons of a given wavelength into directions that lie on a cone centered around the pump-beam axis. The opening angle of the cone is, in our case, a monotonic rising function of the wavelength [9]. In the degenerate case the two photons of the same wavelength are emitted into one cone in opposite directions.

The quantum state of down-conversion photon pairs can be described as two-photon wave packets, showing strong spectral anticorrelation of the single-photon components [3]. In our experiment the down-conversion photons were launched into the single-mode fiber inputs of integrated multiport beam splitters. In terms of these two spatial modes k and l the highly entangled two-photon state can be written as

$$|\psi\rangle = \int\int d\omega' d\omega'' \xi(\omega',\omega'')[|k,\omega'\rangle_1|l,\omega''\rangle_2 + |l,\omega'\rangle_1|k,\omega''\rangle_2], \quad (1)$$

with

$$\xi(\omega',\omega'') \propto \sqrt{\Delta_\epsilon(\omega'+\omega''-\omega_p)} f_{\omega_c'}(\omega') f_{\omega_c''}(\omega''). \quad (2)$$

Here $|k,\omega'\rangle_1$ denotes the state of photon one in mode k with frequency ω'. Δ_ϵ is a sharply peaked function that describes energy conservation in the process of parametric down conversion and approaches Dirac's δ distribution for perfect energy correlation. The filter functions $f_{\omega_c'}(\omega')$ and $f_{\omega_c''}(\omega'')$ describe the spectral distribution of the single-photon components.

A lossless $2N$-port can be represented by a unitary $N\times N$ matrix, where the matrix element M_{ik} is the complex probability amplitude for detecting a particle in output i that has entered the multiport through input k. When two photons are incident on different inputs k and l, as in our experiment, there are two possible evolutions or paths of the system resulting in the joint detection of one photon in output i and the other in output j. These two paths have the probability amplitudes $(M_{ik}M_{jl})$ and $(M_{il}M_{jk})$.

Feynman's rules can be used to obtain the probability P_{ij}^{kl} of detecting one photon in output i and one in a different output j when the two photons entered through different inputs k and l [10]. In the case of classically distinguishable particles the sum of the absolute squares of the amplitudes for all possible paths gives the classical probability

$$P^{(\mathrm{cl})kl}_{ij} = |M_{ik}M_{jl}|^2 + |M_{il}M_{jk}|^2. \quad (3)$$

If, however, the particles are indistinguishable we have to take the absolute square of the sum of all amplitudes that

contribute to a certain outcome. For bosons this results in the quantum-mechanical probability $P^{(\mathrm{QM})kl}_{ij}$ that may show destructive interference:

$$P^{(\mathrm{QM})kl}_{ij} = |M_{ik}M_{jl} + M_{il}M_{jk}|^2 = |M_{ik}M_{jl}|^2 + |M_{il}M_{jk}|^2 + 2\,\mathrm{Re}[(M_{ik}M_{jl})^*(M_{il}M_{jk})]. \quad (4)$$

Photons can be distinguished by their wavelength, polarization, or arrival time at the multiport. In our experiment the wavelengths (within a certain bandwidth) and polarizations of the two photons were the same. By changing the arrival time lag between the two photons at the multiport we were able to vary the degree of distinguishability of the two particles, thus going from the classical to the quantum regime.

In the previous calculation we have not yet evaluated the frequency integrals [Eq. (1)]. These integrals have been shown [2,3] to yield the following expression for the probability:

$$P^{kl}_{ij} = |M_{ik}M_{jl}|^2 + |M_{il}M_{jk}|^2 + 2\,\mathrm{Re}[(M_{ik}M_{jl})^*(M_{il}M_{jk})]\Phi. \quad (5)$$

Φ is called the overlap integral and describes the degree of distinguishability of the two photons. It is defined by

$$\Phi = \int\int d\omega' d\omega'' \xi^*(\omega', \omega'')\xi(\omega'', \omega'). \quad (6)$$

For photons produced in parametric down conversion, which are wavelength selected by interference filters of Gaussian spectral distribution, the overlap integral gives [3]

$$\Phi = \exp\left(-\frac{\omega_d^2 t_c^2}{8}\right)\exp\left(-\frac{2\tau_{\mathrm{in}}^2}{t_c^2}\right), \quad (7)$$

where $\omega_d = \omega_c'' - \omega_c'$ is the difference between the center frequencies of the Gaussian spectral distributions, t_c the coherence time, which is the reciprocal value of the filter bandwidth, and $\tau_{\mathrm{in}} = \Delta x/c$ the time lag between the arrivals of the two photons at the multiport. The characteristic time scale is given by the coherence time t_c, corresponding to a coherence length of $l_c = ct_c$. As τ_{in} goes to zero the two photons become indistinguishable in their arrival time at the multiport. Consequently the photons obey the statistical properties of Bose-Einstein particles, which tend to bunch into one state, i.e., one output port. This bunching leads to a decrease in the coincidence rate between different outputs (anticoincidence) described by the minimum of the pair detection probability P^{kl}_{ij}.

Depending on the phases of the multiport matrix elements in the last term of Eq. (5), the opposite effect of enhanced coincidence between certain output ports can be observed [11]. However, in contrast to higher ($N \geq 4$) dimensional multiports, 2×2 and 3×3 multiports have no phases which are independent of the intensity division ratios. Therefore only bunching into an output port is observed.

The visibility of the second-order interference pattern can be defined using the probabilities P_0 for $\tau_{\mathrm{in}} = 0$ (quantum-mechanically indistinguishable particles) and P_∞ for $\tau_{\mathrm{in}} \to \infty$ (classically distinguishable). Using Eqs. (5) and (7) we get

$$V^{kl}_{ij} = \left|\frac{P_\infty - P_0}{P_\infty}\right| = \left|\frac{2\,\mathrm{Re}[(M_{ik}M_{jl})^*(M_{il}M_{jk})]}{|M_{ik}M_{jl}|^2 + |M_{il}M_{jk}|^2} e^{-\omega_d^2 t_c^2/8}\right|. \quad (8)$$

As we cannot vary the matrix elements in our setups, the visibility depends only on the difference of the center frequencies ω_d. For narrow bandwidths a mismatch in center wavelengths of $\Delta\lambda = 1$ nm at 702 nm in connection with a coherence length of $l_c = 200$ μm would already halve the visibility. Any polarization mismatch, which we have not accounted for in our calculation, of course would also lower the observed visibility.

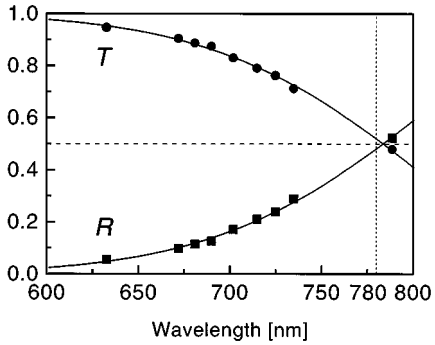

FIG. 1. Intensity transmittance $T = t^2$ and reflectance $R = r^2$ of the integrated fiber beam splitter as functions of the wavelength. Error bars are smaller than symbols and were thus omitted. The fit curves were obtained with a simple model for two coupled waveguides. The fiber couplers had been designed to provide 50-50 splitting at 780 nm.

II. THE SPLITTER EXPERIMENT

In the special case of a lossless four-port the matrix M can be written in terms of the real amplitude transmission and reflection coefficients r and t, because all possible phases can be taken into account by external phase factors:

$$M^{(2)} = \begin{pmatrix} t & r \\ r & -t \end{pmatrix}. \quad (9)$$

From this matrix we can obtain the visibility V^{12}_{12} of the two-photon interference:

$$V^{12}_{12} = \frac{2r^2t^2}{r^4 + t^4} e^{-\omega_d^2 t_c^2/8}. \quad (10)$$

In our experiment we first measured the power division ratio of our fused 2×2 fiber coupler as a function of the wavelength using various light sources (Fig. 1). The single-mode coupler was designed to operate with symmetric power division ratio at 780 nm. At the center wavelength (degenerate case) of our down-conversion source (702 nm) we still expected to work in the single-mode regime, which was justified by our observations. The division ratio, however, was

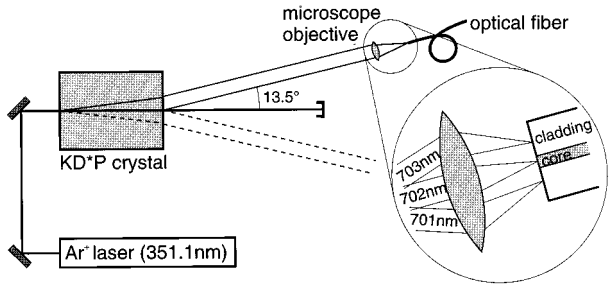

FIG. 2. A lens and a single-mode fiber act as a narrow spectral filter when used in combination with a parametric down-conversion source. The bandwidth, 1 nm in our experiment, depends on the focal length of the microscope objective and the mode-field diameter of the fiber. The angles in the inset are greatly exaggerated for clarity.

strongly asymmetric in terms of the transmitted and reflected light beams. From our measurements we determined the beam splitter matrix:

$$M_{\mathrm{expt}}^{(2)}=\begin{pmatrix} 0.91 & 0.41 \\ 0.41 & -0.91 \end{pmatrix}, \tag{11}$$

with errors in the matrix elements less than 2%. The maximum expected visibility of the two-photon interference for this matrix is $V_{12}^{12}=(39.0\pm 2.5)\%$, assuming zero mismatch in the center frequencies.

Coupling light into single-mode fibers using microscope objectives is equivalent to spatial filtering with pinholes, because only one spatial mode can propagate in the fiber (Fig. 2). In connection with a type-I parametric down-conversion source emitting different wavelengths into different directions, this spatial filter acts as a wavelength selector. We roughly estimated the equivalent filter bandwidth by dividing the mode-field diameter of 5 μm in the fiber by the focal length of the coupling lens (8.3 mm, M20) giving an angular resolution of 0.6 mrad. Using the calculated wavelength dependence of the emission angle from the crystal this results in a bandwidth of approximately 1.5 nm, which is considerably smaller than the 5 nm full width at half maximum (FWHM) of our interference filters. The collected beam had a diameter of 1.5 mm, which was increased to 5.1 mm in later measurements by using M4 objectives.

Figure 3 shows the complete experimental setup of the beam splitter experiment. We used an argon-ion laser at $\lambda=351.1$ nm to pump a deuterated potassium dihydrogen phosphate (KD*P) crystal. The down-conversion photons of the degenerate wavelength 702 nm were selected by interference filters (702 nm center, 5 nm FWHM). We introduced cutoff filters (RG630) to absorb fluorescent and background light. Using M20-microscope objectives, the entangled photons were launched into the two input fibers of the 2×2 coupler. One of the coupling stages was mounted on a motorized micropositioner moving the stage along the emission direction of the entangled photons with a resolution of 0.1 μm. Adjusting the direction of movement for constant photon count rates we made sure that there was no transverse motion, which would have caused a change in the photon wavelength coupled into the fiber. By moving the whole coupler we were then able to scan the photon path-length difference Δx to the beam splitter, thus changing the arrival time difference between the two entangled photons. The polarization state of one of the interfering fields was adjusted using a manual in-fiber polarization controller. The outputs of our beam splitter were attached by mechanical splices to fiber-pigtailed silicon avalanche photodiode (Si-APD) single-photon detectors operating in the Geiger mode. Finally, the electric pulses were fed into the coincidence counting electronics with a coincidence window of 20 ns. As the distance of the stage from the crystal was scanned over approximately 1 mm a computer monitored the singles and coincidence rates and recorded the interference pattern.

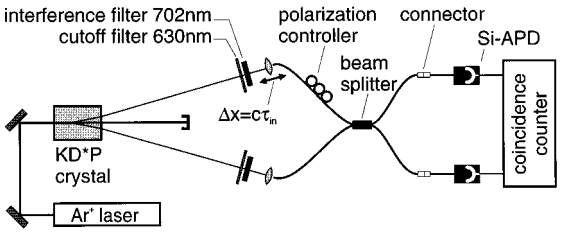

FIG. 3. Experimental setup for measuring the two-photon statistics at a fiber beam splitter. The entangled photons were launched into the two inputs using standard M20-microscope objectives. Silicon avalanche photodiodes (Si-APD) were used as single-photon detectors. Coincidence rates between the two outputs were recorded as functions of the position of the moving input coupler.

In order to determine the optimal parameters for a maximum launch efficiency of the down-conversion light into the single-mode fibers we used a ''reverse-illumination'' scheme. We disconnected the detectors and coupled a laser in reverse direction into the multiport: by measuring the divergence of the emerging beams at the former inputs we were able to precisely tune the focus of our lens, achieving a highly collimated beam and therefore high quality **k** selection. Despite the very narrow spectral distribution we had relatively high coincidence count rates of several 100 counts/s, with zero background counts. The collection efficiency at the fiber inputs could be enhanced in future experiments by using index-matching fluid between lens and fiber, fibers with integrated lenses, systems where the fiber is directly attached to the nonlinear crystal, or even down conversion in nonlinear media inside the fiber.

After reconnecting the detectors no more adjustment was necessary except for the setting of the polarization controller. In this procedure we tried to minimize the coincidence rate at the position of the dip by tilting the three disks of the manual polarization controller.

The experimental results are shown in Fig. 4. The data and the Gaussian fit show that the measurements are very close to the maximum theoretically possible value for the visibility. Assuming perfect polarization adjustment even a difference in the center wavelengths as small as 0.4 nm can explain the difference between theoretical and experimental values. The observed coherence length was 190 ± 4 μm, corresponding to a bandwidth of 1.0 nm. The following table compares the theoretical maximum with the experimental visibility:

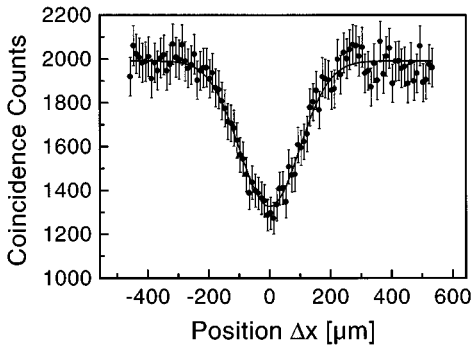

FIG. 4. Coincidences in 10 s between the two output ports of the fiber beam splitter as a function of the position of the input coupler, which is equivalent to the path-length difference of the two entangled photons from the source to the beam splitter. The two-photon interference leads to a bunching of photons into either output mode which causes the dip in the coincidence rate. The visibility was $V_{12}^{12}=(34\pm1)\%$. The width of the Gaussian dip, $\Delta x_{\mathrm{FWHM}}=222\pm6\ \mu$m, corresponds to a coherence length of $l_c=190\pm4\ \mu$m.

Theoretical max.	39.0%
Experiment	$(34.0\pm1.0)\%$

III. THE TRITTER EXPERIMENT

In our second experiment we investigated the case of an integrated six-port (tritter). We expected the transmittances (diagonal terms) to be equal but to be different from the reflectances (off-diagonal terms). The matrix of our six-port with diagonal elements of modulus $|t|$ and off-diagonal elements of modulus $|r|$ thus is symmetric and can be written as follows:

$$M^{(3)}=\begin{pmatrix} t & r & r \\ r & te^{i2\varphi} & re^{i\varphi} \\ r & re^{i\varphi} & te^{i2\varphi} \end{pmatrix}. \tag{12}$$

Again, all other phases are accounted for by external phase factors. The remaining internal nontrivial phase φ of the tritter matrix is determined from the moduli of the matrix elements to fulfill the unitarity condition for M:

$$\cos(\varphi)=-r/2t. \tag{13}$$

The six-port was fabricated for symmetric operation at 780 nm. Measurements of the intensity division matrix at our wavelength (702 nm) showed that all diagonal elements were equal within the achieved accuracy, which justified the assumptions that led to Eq. (12). From these measurements we determined the amplitude matrix of our 3×3 coupler to be

$$M_{\mathrm{expt}}^{(3)}=\begin{pmatrix} 0.80 & 0.43 & 0.43 \\ 0.43 & 0.80e^{i0.83\pi} & 0.43e^{i1.41\pi} \\ 0.43 & 0.43e^{i1.41\pi} & 0.80e^{i0.83\pi} \end{pmatrix}, \tag{14}$$

with errors in the moduli and phases less than 2%. The maximum possible visibilities calculated from Eq. (8) are then $V_{12}^{12}=(46.0\pm3.0)\%$ and $V_{13}^{12}=V_{23}^{12}=(22.0\pm1.4)\%$.

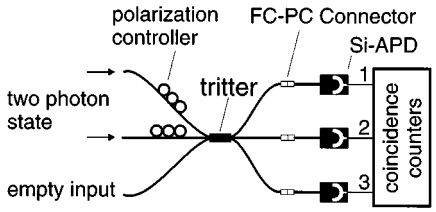

FIG. 5. Part of the experimental setup for measuring the two-photon statistics at a fiber six-port. The remaining setup is identical to that in Fig. 3. The entangled photons from the parametric down-conversion crystal were launched into two of the three inputs. Coincidence counters recorded coincidence rates between all three pairs of outputs.

The experimental setup of Fig. 3 was modified as shown in Fig. 5. In this case we connected the tritter outputs to the detectors with FC/PC connectors instead of mechanical splices and used two instead of one polarization controller for polarization adjustment. Coincidence counters registered coincidences between any two of the three detectors (Fig. 5). Otherwise, the procedure of optimizing the launch of the down-conversion photons and adjusting the polarization was the same as in the beam splitter experiment.

The experimental results are shown in Fig. 6. The three curves and the Gaussian fit again show that the measurements approach the maximum theoretically possible value

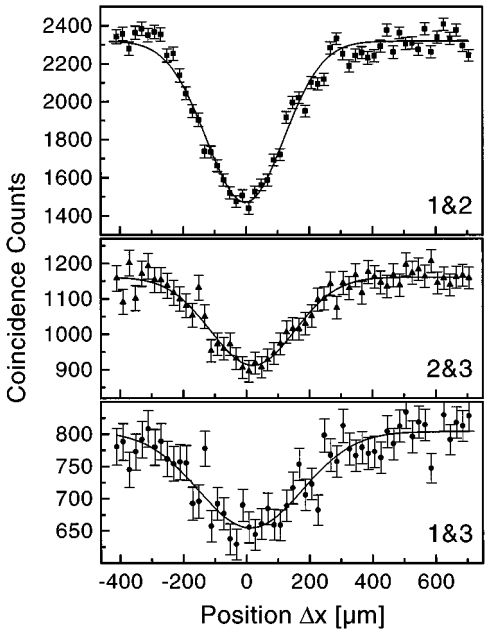

FIG. 6. Coincidence counts in 10 s between the output ports of the integrated fiber tritter as a function of the position of the input coupler. The count rates were corrected for a linear drift of the effective laser power, with the actual coincidence rates at $\Delta x=-400$ as reference. Again the rates show dips as the path-length difference goes to zero. The visibilities of the dips were $V_{12}^{12}=(40\pm1)\%$, $V_{13}^{12}=(22\pm2)\%$, and $V_{23}^{12}=(20\pm2)\%$, where the upper indices denote the inputs and the lower indices the measured outputs of the tritter. The width of the coincidence dip between outputs 1 and 2 was $\Delta x_{\mathrm{FWHM}}=300\pm10\ \mu$m, corresponding to a coherence length of $l_c=255\pm9\ \mu$m.

for the visibility. The observed coherence length was 255 ± 9 μm, corresponding to a filter bandwidth of 0.7 nm. The following table summarizes the results of the two-photon interference experiment at the fiber six-port.

	V_{12}^{12}	V_{13}^{12}	V_{23}^{12}
Theoretical max.	0.46	0.22	0.22
Experiment	$(40 \pm 1)\%$	$(22 \pm 2)\%$	$(20 \pm 2)\%$

IV. CONCLUSION AND OUTLOOK

The experiments presented herein clearly show that fused fiber couplers not only act as power dividers but also provide coherent beam splitting on individual quanta. Their action on entangled photon pairs shows that the rather complex photon propagation mechanism in the multiport can be reduced to the few complex parameters of a unitary matrix. These couplers permit the realization of complex quantum interferometers for the simulation of higher dimensional spin systems. This could make possible experimental realizations of Greenberger, Horne, and Zeilinger [14] schemes or other tests of Bell inequalities in higher dimensional Hilbert spaces.

As a next step we are currently applying the integrated fiber tritter in a three-path Franson-Bell-type experiment [12,13]. In that experiment entangled photons from a down-conversion source are coupled into two separate three-path Mach-Zehnder interferometers. Each of the two interferometers consists of two fiber tritters, where the outputs of the first tritter are coupled to the inputs of the second one by a short, a medium, and a long path. As the phases inside the interferometers are changed, coincidence measurements between the three outputs of one of the interferometers and the three outputs of the other one reveal nonlocal-nonclassical interferences [15].

ACKNOWLEDGMENTS

This work was supported by the Fonds zur Förderung der wissenschaftlichen Forschung (Austrian Science Foundation), Schwerpunkt Quantenoptik, Projekt S6502. G.W. acknowledges financial support from the Austrian Academy of Sciences.

[1] C. K. Hong, Z. Y. Ou, and L. Mandel, Phys. Rev. Lett. **59,** 2044 (1987).
[2] H. Fearn and R. Loudon, J. Opt. Soc. Am. B **6,** 917 (1989).
[3] R. A. Campos, B. E. A. Saleh, and M. C. Teich, Phys. Rev. A **42,** 4127 (1990).
[4] J. Breguet, A. Muller, and N. Gisin, J. Mod. Opt. **41,** 2405 (1994).
[5] J. D. Franson and H. Ilves, Appl. Opt. **33,** 2949 (1994).
[6] P. R. Tapster, J. G. Rarity, and P. C. M. Owens, Phys. Rev. Lett. **73,** 1923 (1994).
[7] A. Muller, H. Zbinden, and N. Gisin, Nature (London) **378,** 449 (1995).
[8] G. Weihs, M. Reck, H. Weinfurter, and A. Zeilinger, Opt. Lett. **21**, 302 (1996).
[9] This is not the case for type-II down conversion; see, for example, P. G. Kwiat, H. Weinfurter, A. Zeilinger, A. V. Sergienko, and Y. Shih, Phys. Rev. Lett. **75,** 4337 (1995).
[10] R. P. Feynman, R. Leighton, and M. Sands, *The Feynman Lectures on Physics* (Addison-Wesley, Reading, MA, 1965), Vol. III.
[11] K. Mattle, M. Michler, H. Weinfurter, A. Zeilinger, and M. Zukowski, Appl. Phys. B **60,** S111 (1995).
[12] J. D. Franson, Phys. Rev. Lett. **62,** 2205 (1989).
[13] A. Zeilinger, M. Zukowski, M. Horne, J. H. Bernstein, and D. M. Greenberger, in *Proceedings of the Adriatico Workshop on Quantum Interferometry*, edited by F. DeMartini, G. Denardo, and A. Zeilinger (World Scientific, Singapore, 1993), pp. 159–169.
[14] D. M. Greenberger, M. A. Horne, and A. Zeilinger, in *Bell's Theorem, Quantum Theory, and Conceptions of the Universe*, edited by M. Kafatos (Kluwer Academic, Dordrecht, 1989), pp. 69–72.
[15] M. Reck and A. Zeilinger, in *Proceedings of the Adriatico Workshop on Quantum Interferometry*, edited by F. De Martini, G. Denardo, and A. Zeilinger (World Scientific, Singapore, 1993), pp. 171–177.